Onset of laminar separation and vortex shedding in flow past unconfined elliptic cylinders

Cite as: Phys. Fluids **26**, 023601 (2014); https://doi.org/10.1063/1.4866454
Submitted: 21 May 2013 . Accepted: 07 February 2014 . Published Online: 27 February 2014

Immanuvel Paul, K. Arul Prakash, and S. Vengadesan

PHYSICS OF FLUIDS **26**, 023601 (2014)

Onset of laminar separation and vortex shedding in flow past unconfined elliptic cylinders

Immanuvel Paul,[a] K. Arul Prakash, and S. Vengadesan
Department of Applied Mechanics, Indian Institute of Technology Madras, Chennai-600036, India

(Received 21 May 2013; accepted 7 February 2014; published online 27 February 2014)

This article presents the numerical studies on predicting onset of flow separation and vortex shedding in flow past unconfined two-dimensional elliptical cylinders for various Axis Ratios (AR) and a wide range of Angles of Attack (AOA). An efficient Cartesian grid technique based immersed boundary method is used for numerical simulations. The laminar separation Reynolds number (Re_s) that marks separation of flow from surface and the critical Reynolds number (Re_{cr}) which represents transition from steady to unsteady flow are determined using diverse methods. A stability analysis which uses Stuart-Landau equation is also performed for calculating Re_{cr}. The shedding frequency (St_{cr}) that corresponds to Re_{cr} is calculated using Landau constants. The simulated results for circular cylinder are found to be in good agreement with the literature. The effects of AR and AOA on Re_s, Re_{cr}, and St_{cr} are studied. It is observed that the Re_s, Re_{cr}, and St_{cr} exhibit a direct/inverse relationship with AR depending upon the given AOA. Correlations of Re_s, Re_{cr}, and St_{cr} with respect to AR and AOA are proposed with good accuracy. © *2014 AIP Publishing LLC*. [http://dx.doi.org/10.1063/1.4866454]

I. INTRODUCTION

Fluid flow over a streamlined/bluff body usually exhibits a rich set of flow physics. Dimensional analysis revealed that these flows are characterized by a single dimensionless parameter, Reynolds number (Re). Re is the ratio of inertial forces to viscous forces and it is defined as $Re = U_\infty d_H/\nu$, where U_∞ and d_H are the velocity and length scales. When fluid passes over an arbitrarily shaped body, boundary layer is developed on the surface of the body. This boundary layer and its stability cause significant changes to flow characteristics. For very low Re, the boundary layer remains attached to the body. However, when Re is increased to a particular value, the boundary layer gets detached from the surface, and forms a closed loop in the immediate downstream of the body.[1] The Re at which the flow separates from the surface is termed as laminar separation Reynolds number (Re_s). The concept of separation is an interesting fluid mechanics phenomena, and a range of analytical, experimental, and numerical techniques can be found in the literature to estimate Re_s. A recent article by Sen *et al.*[30] compares the values of Re_s for circular cylinder predicted by different authors through different techniques. They reported a large scatter in the literature values of Re_s.

As Re is increased beyond Re_s, the separated boundary layer starts shedding periodically from top and bottom surfaces of the body. This periodic shedding of vortices gives rise to the appearance of the so called "von-Karman vortex street" in the downstream of the body. Thus, a steady flow is bifurcated into an unsteady flow. The Re at which this bifurcation occurs is termed as critical Reynolds number (Re_{cr}) and the vortex shedding frequency caused by this transition is termed as critical Strouhal number (St_{cr}). Zielinska *et al.*[3] analyzed the mean velocity profiles of the unsteady wake and showed that the mean oscillatory flow is the result of nonlinear coupling between the basic

[a]immanuvelpaul@gmail.com

flow and the fundamental unstable mode. From the literature, it is observed that the value of Re_{cr} for flow past circular and square cylinder is in the range of 47–50.[1]

Unsteady forces start to act on the body when the flow alters from steady to unsteady. As a result, the transition causes vibrations on the body.[4] Therefore, it is imperative to know the onset of bifurcation (i.e., Re_{cr}) and the magnitude of shedding caused by the bifurcation (i.e., St_{cr}) *a priori* for a given flow condition. The literature reveals that the prediction of Re_{cr} and St_{cr} have been performed theoretically,[5] experimentally,[6–10] and numerically[5,11–13] for flow around circular cylinders. Sohankar *et al.*[14] determined the values of Re_{cr} and St_{cr} for flow past square cylinders at different angles of attack (AOA). Their study reported a decrease in both Re_{cr} and St_{cr} for increasing AOA. There are also some studies on the effect of blockage ratio on onset of vortex shedding from circular cylinders.[12,15] However, literature on predicting the onset of vortex shedding for elliptic cylinder is very limited. Jackson[11] carried out stability analysis to predict the onset of vortex shedding for confined flow past different body shapes like ellipse, triangle, and prisms. It was observed that Re_{cr} is sensitive to blockage ratio.

From the discussed literature, it is observed that most of the studies concentrated on onset of separation and vortex shedding in flow past circular, square, and confined elliptic cylinders. On the other hand, many of the engineering applications such as flow past wings, missiles, and heat exchanger tubes require the problem to be modeled as unconfined flow past elliptic cylinders. In flow past elliptic cylinders, many parameters like Axis Ratio (AR) which is defined as the ratio of major to minor axes, AOA, and Reynolds number (Re) greatly influence the flow behavior. Circular cylinder is a form of elliptic cylinder when AR = 1.0. A recent article by Radi *et al.*[16] showed that changing the AR from 0 to 1 for an elliptic cylinder kept at AOA = 0° changes the characteristics of *St-Re* curves. However, the study of onset of separation and vortex shedding for flow past elliptic cylinders is largely unexplored. Sen *et al.*[2] calculated Re_s values for elliptic cylinders of various AR and AOA. Nevertheless, there is no detailed study on the combined effect of AR and AOA on critical parameters such as Re_{cr} and St_{cr} as well as no agreement on Re_s values. This article aims to provide these data. For this purpose, flow past two-dimensional elliptic cylinders of AR = 0.1, 0.4, 0.6, 0.8, and 1.0 are simulated. Here, AR = 0.1 resembles a flat plate, whereas AR = 1.0 represents a circular cylinder. The AOA is varied as 0°, 30°, 45°, 60°, and 90°. Three distinct techniques are used for predicting Re_s: (i) Flow Visualization Method (FVM), (ii) Wake Length Method (WLM), and (iii) Flow Separation Criteria Method (FSCM). Similarly, another three distinct techniques are adopted for calculating Re_{cr} and St_{cr}. They are: (i) FVM, (ii) Saturation Amplitude Analysis (SAA), and (iii) Hopf Bifurcation Analysis (HBA). The details of these methods will be discussed in Secs. V and VI. The Re_s, Re_{cr}, and St_{cr} are computed using these techniques and the values are compared. Stuart-Landau equation is solved numerically to obtain Landau constants.

II. GOVERNING EQUATIONS AND NUMERICAL METHODOLOGY

In this paper, Computational Fluid Dynamics (CFD) is used to predict Re_s, Re_{cr}, and St_{cr}. In conventional CFD approach, a surface grid which confronts to the solid surface is generated first. Based on boundary condition applied on the surface grid, a volume grid which covers the fluid domain is generated next. The physical problem discussed in this article requires a new grid to be generated for every case (because of AR and AOA) which is time consuming and computationally demanding. In order to avoid this, Immersed Boundary Method (IBM) is used in this present study. In IBM, volume grid (an Eulerian grid) is generated first and then the solid body is immersed in the fluid domain through a set of Lagrangian marker points. Thus, the Eulerian grid is used for the fluid domain and the Lagrangian marker points are used to represent the solid body. Interaction between Eulerian domain and Lagrangian marker points is achieved through a Dirac delta function. The solid body is modeled by a forcing term which is added to the governing equations of flow. Thus, the governing equations of fluid flow around an arbitrarily shaped body in vector form for IBM are

$$\nabla \cdot \boldsymbol{u} = 0, \tag{1}$$

$$\frac{\partial \boldsymbol{u}}{\partial \tau} + (\boldsymbol{u} \cdot \nabla)\,\boldsymbol{u} = -\nabla p + \frac{1}{Re}\nabla^2 \boldsymbol{u} + \boldsymbol{f}, \tag{2}$$

where $\boldsymbol{u}$ is the non-dimensional velocity vector ($\boldsymbol{u} = u/u_\infty$, u – dimensional velocity vector in m s^{-1}, u_∞ – free stream velocity in m s^{-1}), p is the non-dimensional pressure ($p = \mathrm{p}/\rho u_\infty^2$, p – dimensional pressure in N/m^2, ρ – dimensional density in kg/m^3), and τ is non-dimensional time ($\tau = t_t u_\infty/d_H$, t_t = dimensional time in s and d_H is hydraulic diameter which is defined as $d_H = 4A/P$, A is the area and P is the perimeter of the elliptic cylinder). The Reynolds number (Re) is defined as $Re = \rho u_\infty d_H/\mu$, where μ – viscosity of fluid. Hydraulic diameter (d_H) is taken as the characteristic length. The additional term in Eq. (2) ($\boldsymbol{f}$) is known as forcing function which is used to model the solid body in fluid domain.

The governing equations are solved on a Cartesian grid using projection method based on IBM which uses a finite difference discretization on a staggered grid. To impose boundary conditions on solid body, singular forces are applied on each Lagrangian marker point in such a way that, forcing will result in enforcement of required boundary condition. These singular forces are then distributed to the nearby Eulerian points so that the presence of solid body will be felt in the fluid domain. Thus, the singular forces applied on Lagrangian marker points determine the forcing term.

The algorithm and validation of the code are reported for circular and elliptic cylinders in Sudhakar and Vengadesan[17] and Raman *et al.*,[18] respectively. The same algorithm is extended for studying natural convection from an elliptic cylinder in an enclosure by Raman *et al.*[19] and for forced convective heat transfer from elliptic cylinders by Paul *et al.*[20]

III. COMPUTATIONAL DOMAIN AND GRID DETAILS

The computational domain along with the boundary conditions is depicted in Figure 1. An uniform streamwise velocity profile and fully developed flow conditions are imposed at the inlet and outlet of the computational domain, respectively. The top and bottom sides of the computational domain are considered as free-slip walls. The two-dimensional elliptic cylinder is discretized with 315 Lagrangian marker points. The size of the computational domain is chosen as $-8d_H \le x \le 25d_H$, $-8d_H \le y \le 8d_H$. The Eulerian domain is discretized with a non-uniform grid with 381 and 299 grid points along x and y directions, respectively. An uniformly spaced grid is embedded around the elliptic cylinder for the effective use of Dirac delta function. The size of the uniform grid sized computational domain is ($-1.0d_H \le x \le 1.0d_H$, $-1.0d_H \le y \le 1.0d_H$) with the mesh size of $\Delta x = \Delta y = 0.01$ (obtained using grid independence study).

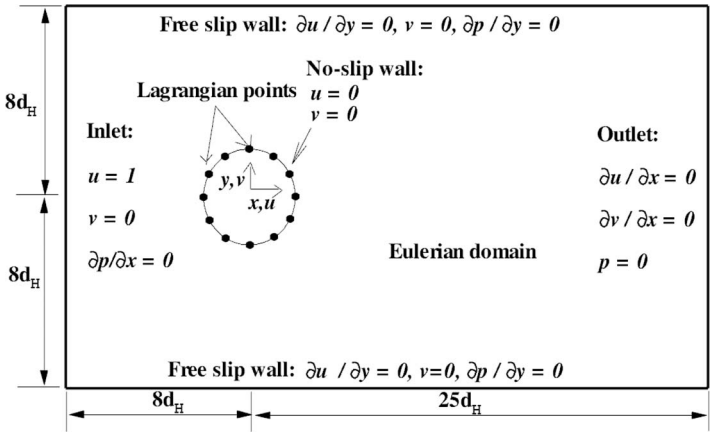

FIG. 1. Computational domain with boundary conditions.

TABLE I. Comparison of L/d_H and θ_s obtained using different mesh sizes Δx.

	$Re = 30$		$Re = 40$	
Δx	L/d_H	θ_s	L/d_H	θ_s
0.04	2.995	129.003	4.661	127.108
0.025	2.984	129.098	4.652	127.120
0.01	2.982	129.120	4.647	127.128
0.005	2.980	129.126	4.645	127.126

TABLE II. Comparison of $C_{L_{rms}}$ with the literature for flow around circular cylinder.

Re	Norberg[26]	Present study
50	0.034	0.035
100	0.233	0.234
150	0.361	0.369
200	0.457	0.461

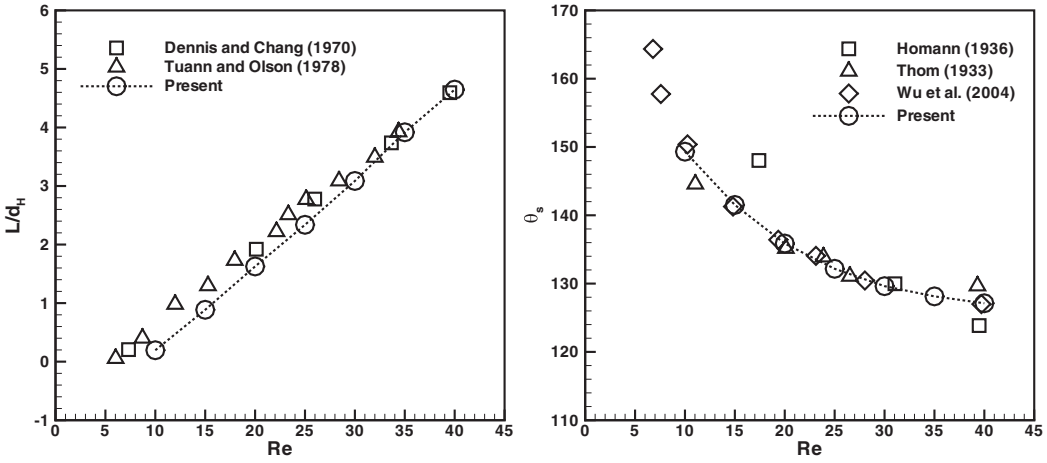

(a) (b)

FIG. 2. Comparison of L/d_H and θ_s with the literature values for flow around circular cylinder: (a) Wake length, (b) separation angle.

IV. GRID INDEPENDENCE AND VALIDATION STUDIES

Meshes with different values of $\Delta x = 0.04$, 0.025, 0.01, and 0.005 are generated for grid independence study, and flow over a circular cylinder is simulated at $Re = 30$ and 40. The values of wake length (L/d_H) and separation angle (θ_s) for each case is compared in Table I. From Table I, it is observed that there is not much variation in the value L/d_H and θ_s after $\Delta x = 0.01$.

Now, the solver is validated for steady flow around circular cylinder. Comparison of simulated values of L/d_H and θ_s with the literature results are shown in Figures 2(a) and 2(b), respectively. It is observed from the figures that the present simulation results are in good agreement with the available literature values of L/d_H[21,22] and θ_s.[23–25] Values of $C_{L_{rms}}$ are considered for the validation of unsteady case, and the present study is found to be matching with the literature[26] as shown in Table II. Some more grid independence studies and unsteady case validations pertaining to fluid flow around inclined elliptic cylinders (C_{d_av} and *St*) using this algorithm can be found in Paul[27] and Paul *et al.*[28]

V. CALCULATION OF LAMINAR SEPARATION REYNOLDS NUMBER

A. Flow visualization method

Streamline patterns are utilized to predict Re_s in this method. Simulations are initially performed from $Re = 1$ in steps of 1. For every Re, the streamline pattern is analyzed. For symmetric bodies, separation is identified by a set of counter-rotating attached vortices behind the cylinder. This well-established concept is applied for circular cylinder as shown in Figure 3(a) where closed loop vortices are first observed at $Re = 7$. Therefore, the Re_s for circular cylinder is found out to be 6.5 ± 0.5.

This method is now extended to asymmetric elliptic cylinders as shown in Figure 3(b) for the case: AR $= 0.1$ kept at 30°. It can be seen from the figure that at $Re = 21$, the flow leaves the surface smoothly while at $Re = 22$, a small single recirculation vortex is observed over the leeward surface of the cylinder. As a consequence, Re_s for AR $= 0.1$ and AOA $= 30^\circ$ is determined as $Re_s = 21.5 \pm 0.5$. This single recirculation bubble which marks the separated flow in asymmetric body is remarkably different from closed loop vortices for the symmetric body. Formation of this kind of single recirculation bubble also supports the earlier observation by Park *et al.*[29]

B. Wake length method

It is known that once the flow separated from the surface, it forms a separated flow region with recirculation behind the cylinder. This separated flow region is known as wake. A typical wake is characterized by its length (L/d_H) which is a measurable quantity. In this article, L/d_H is computed as the horizontal length between the rear stagnation point and zero velocity point in the centerline mean u-velocity profile. A typical wake length measurement using centerline mean u-velocity profile is shown in Figure 4 for flow around circular cylinder. In the figure, the zero velocity points on the mean velocity profile is identified by drawing a constant line of zero velocity value.

Since wake length maintains a linear relationship with Re, it is possible to predict the Re_s by measuring the wake length. The simulations are carried out for a wide range of Re in steps of 1. For every case, the wake length is measured. A least square curve fit is performed on L/d_H-Re curve to

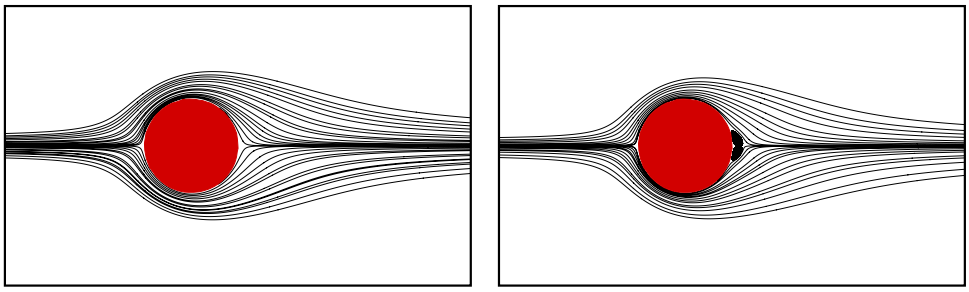

(a)

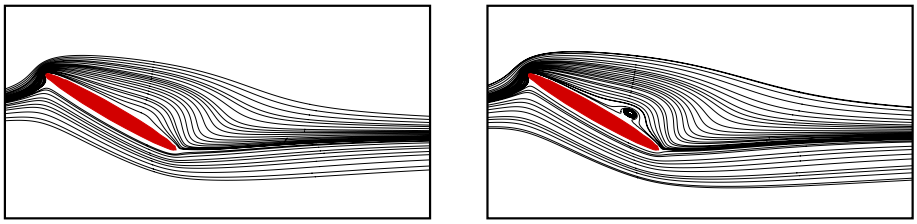

(b)

FIG. 3. Streamline contours of: (a) Circular cylinder (AR $= 1.0$), $Re = 6$ (left), $Re = 7$ (right), (b) AR $= 0.1$, AOA $= 30^\circ$, $Re = 21$ (left), $Re = 22$ (right).

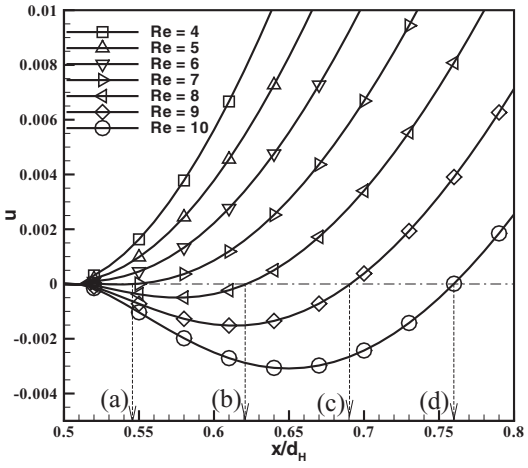

FIG. 4. Measurement of wake lengths from u-velocity profiles for flow around circular cylinder. The numerical values of L/d_H in the figure for (a) 0.0507, (b) 0.1282, (c) 0.1953, (d) 0.2676.

find the Re at which L/d_H becomes zero. This Re is referred as Re_s. This is shown in Figure 5(a) for circular cylinder and Figure 5(b) for elliptic cylinder (AR = 0.4 and AOA = 90°). The predicted value of Re_s for circular cylinder by this technique is 6.27, and it is in good agreement with Sen *et al.*[30] which reported as 6.29. However, the present technique adopted in this study is not robust enough to predict value of Re_s for asymmetric cylinders.

C. Flow separation criteria method

FSCM makes use of an analytical condition derived by Srinivasan[31] in order to calculate Re_s. It was proposed that at Re_s, the value of $\frac{\partial^2 u}{\partial x^2}$ becomes zero at the rear stagnation point. Using this concept, the value of $\frac{\partial^2 u}{\partial x^2}$ for each Re is calculated at the rear stagnation point for circular and symmetric elliptic cylinders. The calculated values of $\frac{\partial^2 u}{\partial x^2}$ are then plotted against Re. The Re at which $\frac{\partial^2 u}{\partial x^2}$ becomes zero is marked as Re_s. For this purpose, the least square curve fit is performed on Re-$\frac{\partial^2 u}{\partial x^2}$ curve as shown in Figure 6(a) for circular, and in Figure 6(b) for elliptic cylinders to mark

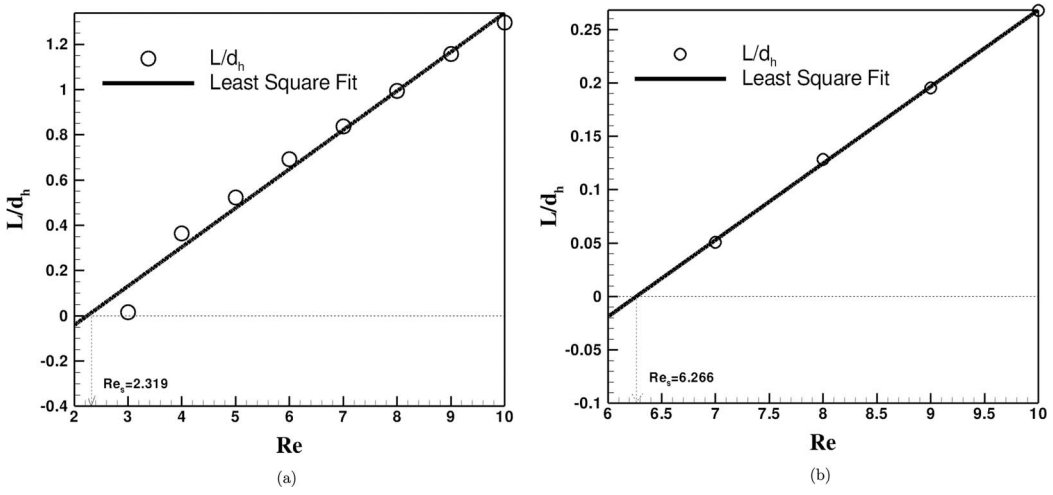

FIG. 5. Wake length method: (a) circular cylinder (AR = 1.0), (b) AR = 0.4 with AOA = 90°.

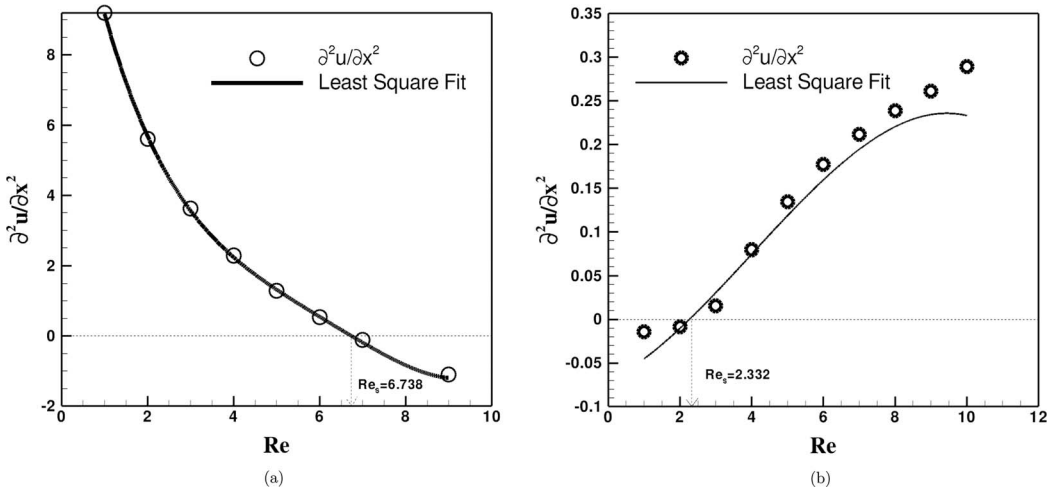

FIG. 6. Flow separation criteria analysis: (a) circular cylinder (AR = 1.0), (b) AR = 0.4 with AOA = 90°.

TABLE III. Comparison of calculated Re_s obtained by FSCM with the literature for AR = 0.8.

AOA (deg)	Sen *et al.*[2]	Present study
0	9.90	7.081
30	10.95	9.843
45	9.46	7.614
60	7.93	5.204
90	4.99	4.977

Re_s. This technique predicts Re_s for circular cylinder as 6.738 which is reasonably matching with the literature value of 6.29 reported by Sen *et al.*[30]

It is interesting to note from the literature that FSCM has been applied only to symmetric elliptic cylinders, and the authors of this present study have now extended this technique to asymmetric cylinders as well. For asymmetric cylinders, the value of $\frac{\partial^2 u}{\partial x^2}$ is calculated at a surface point which coincides with the geometric centerline of the computational domain. The values of Re_s obtained through this method are compared with that of Sen *et al.*[2] in Table III. It is observed from Table III that a considerable amount of discrepancy is observed for results of elliptic cylinder even though a good agreement was obtained for circular cylinder. However, the reliability of the results obtained by FSCM are defended by the results obtained from FVM and WLM as shown in Table VIII.

VI. ESTIMATION OF CRITICAL REYNOLDS NUMBER

A. Flow visualization method

Vorticity contours and streamlines patterns are examined in this method to identify the Re_{cr}. In the first step of this method, for each combination of AR and AOA, simulations are carried out for a sequence of random Reynolds numbers as the *Re* at which the bifurcation occurs is not known *a priori*. At the end of the first set of simulations, shedding range of *Re* is obtained for a given case. This process is explained for circular cylinder as follows. Assuming that there is no information available regarding when the shedding will occur for flow around circular cylinder, the simulations are initially performed for *Re* = 30, 35, 40, 45, 50, 60, 65, 70, and 75. Simulation time is checked whether it is long enough so that all the initial transients would be died and the shedding

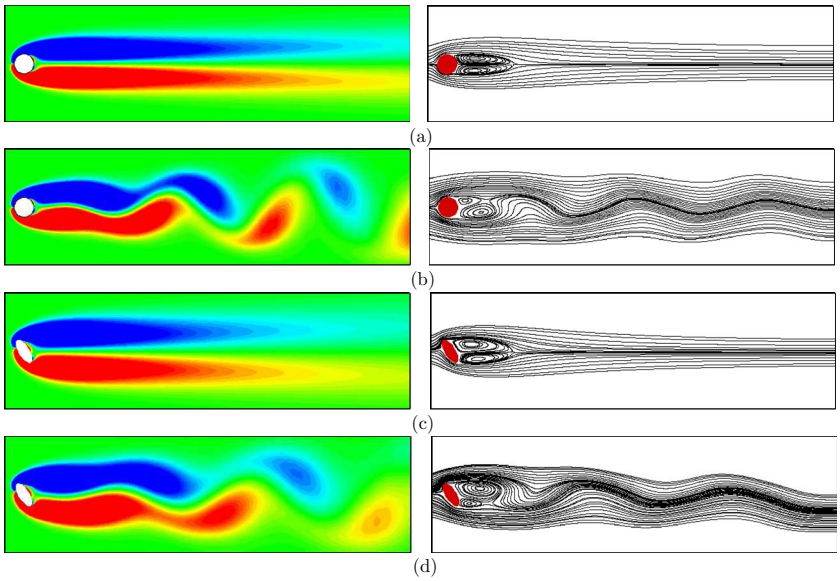

FIG. 7. Instantaneous vorticity contours and streamlines pattern of: (a) Circular cylinder (AR = 1.0), $Re = 48$, (b) AR = 1.0, $Re = 49$, (c) AR = 0.4, AOA = 60°, $Re = 31$, (d) AR = 0.4, AOA = 60°, $Re = 32$. [The contour levels for vorticity are −0.5 (0.1) 0.5.]

pattern is fully periodic. Accordingly, simulations are carried out up to non-dimensional time units of $\tau = 900$.

The vorticity contours and the streamlines patterns are then examined whether shedding is there or not. It is observed for the circular cylinder case that shedding occurs at $Re = 50$ but there is no shedding observed at $Re = 45$. Therefore, the shedding range of Re for circular cylinder is defined as 45–50. Within this shedding Re range, the Re is varied in steps of 1. Vorticity contours are analyzed for the appearance of symmetric bubble behind the cylinder. If there is a symmetric bubble, then the flow is said to be in stable condition. If not, the flow is said to be time dependent. To support the results obtained by vorticity contours, streamlines patterns are analyzed for appearance of alleyways which are instantaneous pathways that appear in the streamlines pattern along which the fluid is drawn from top/bottom side of the cylinder into the circulation region.[32] It is well known that alleyways are formed in streamlines pattern when there is a vortex shedding. This fundamental concept is utilized for streamlines pattern analysis. Typical results are shown in Figure 7 .

The symmetric bubble behind the circular cylinder is observed at $Re = 48$ (Figure 7(a)). The streamlines pattern also supports the vorticity contour result as there is no alleyway visible for $Re = 48$ (Figure 7(a)). This confirms that there is no shedding and the flow is stable at $Re = 48$. When Re is increased to 49, the symmetric bubble disappears in the vorticity contour, and alleyways are visible in the streamlines pattern as depicted in Figure 7(b). This reveals that the flow is unstable and time dependent at $Re = 49$. Since Re has been varied in steps of 1, the Re_{cr} for circular cylinder is 48.5 ± 0.5. Our result for circular cylinder is in good agreement with the literature.[5]

This technique is now applied for flow past elliptic cylinders as shown in Figures 7(c) and 7(d). The Re_{cr} for the combinations AR = 0.4 with AOA = 60° is found out to be 31.5 ± 0.5.

B. Saturation amplitude analysis

In this method, instantaneous lift curves are considered to determine the onset of vortex shedding. When the flow is stable, the amplitude of C_L with respect to time decreases as shown in Figure 8(a). When the flow is fully periodic, the amplitude grows in time and reaches to a saturated value as depicted in Figure 8(b). This value is referred as saturation amplitude (Λ_{sat}). A plot between Re and Λ_{sat}^2 reveals that saturation amplitude grows as Re increases. Therefore, it can be understood that the Re at which Λ_{sat}^2 vanishes corresponds to Re_{cr}. For this purpose, simulations are performed

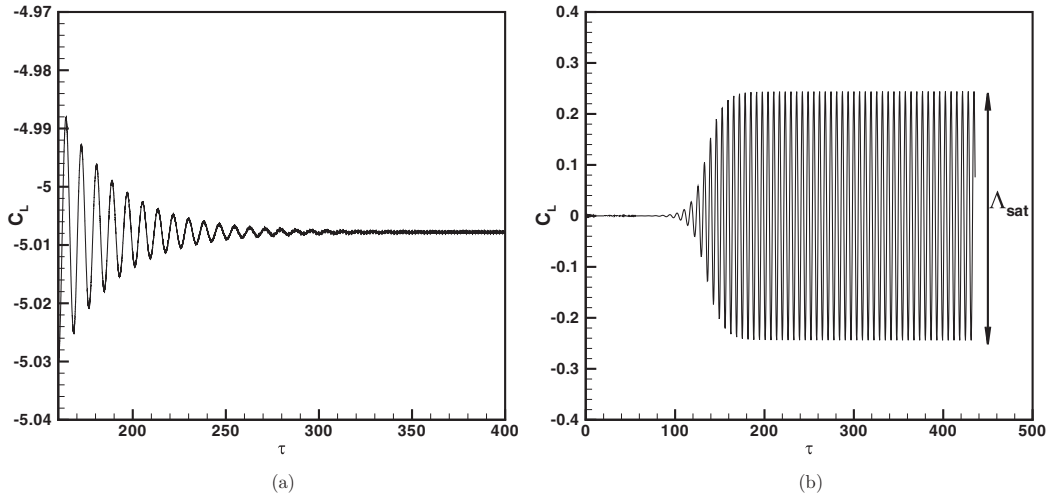

FIG. 8. (a) Signal with decaying amplitude, (b) signal with saturated amplitude (Λ_{sat}).

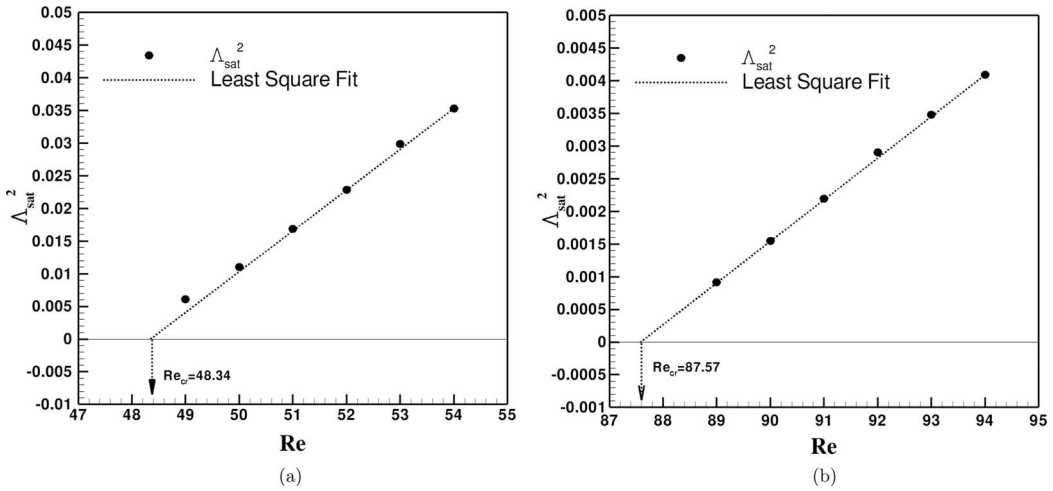

FIG. 9. Saturation amplitude analysis: (a) AR = 1.0, (b) AR = 0.6 with AOA = 0°.

for above the threshold of Re_{cr}. Considering circular cylinder case, the simulations are carried out for Re = 49, 50, 51, 52, and 53. The corresponding Λ^2_{sat} for each case is computed and plotted as a function of Re as shown in Figure 9(a). A least square curve fit as shown as dotted line in Figure 9(a) is performed on the data points. The least square fit curve crosses $\Lambda^2_{sat} = 0$ at 48.34. Therefore, the Re_{cr} for circular cylinder is found to be 48.34 which is in good agreement with the literature.[5] SAA is applied to all the cases considered in this study to predict Re_{cr}. Figure 9(b) shows one such example of how SAA is applied to calculate Re_{cr} for an elliptic cylinder of AR = 0.6 kept at AOA = 0°. The Re_{cr} for this case is calculated as 87.57.

C. Hopf bifurcation analysis

Mathis *et al.*[33] and Sreenivasan *et al.*[6] proved experimentally that the bifurcation which occurs during transition from steady to unsteady flow is of super-critical Hopf bifurcation. The post-critical state of any unstable system which undergoes Hopf bifurcation is effectively modeled by Landau

TABLE IV. Values of Landau constants obtained for transverse velocities taken at different locations at $Re = 49$.

Point	γ	α	ω	β	c_∞	$\Delta\omega$
1	0.007884	0.546	0.8130	−1.3001	−2.381	0.01877
2	0.007841	0.181	0.8111	−0.4246	−2.346	0.01839
3	0.007880	0.171	0.8104	−0.3951	−2.311	0.01821
4	0.007812	0.134	0.7984	−0.3221	−2.404	0.01878
5	0.007897	0.112	0.8014	−0.2675	−2.389	0.01886
6	0.007809	0.384	0.8173	−0.3143	−2.381	0.01859
7	0.007912	0.147	0.8114	−0.3491	−2.377	0.01882
8	0.007831	0.138	0.8087	−0.3196	−2.316	0.01813
9	0.007834	0.176	0.8199	−0.4171	−2.370	0.01856

equation.[34] According to Landau, the evolution equation of any perturbed signal is given as

$$\frac{d(\ln(\Lambda))}{dt} = \gamma - \alpha\Lambda^2, \tag{3}$$

$$\frac{d\theta}{dt} = \omega - \beta\Lambda^2, \tag{4}$$

where γ represents the amplification rate, and ω represents the angular frequency of perturbations having varying amplitudes. These constants are global, in the sense that they are almost constant for the entire computational domain (proved in Table IV). Whereas, the constants α and β are not global. These real constants (γ, ω, α, and β) are known as Landau constants. Computing these constants will give deeper insight to complex flow systems which undergo the super-critical Hopf bifurcation. Equations (3) and (4) are referred as fundamental equations of Landau model. They represent the amplitude and phase evolution of the perturbed signal.

For a system to be stable, $\frac{d\Lambda}{dt}$ (Eq. (3)) should be negative, that is, the amplitude should decay. Therefore, stable condition of a system is defined by $\gamma < 0$ and $\alpha > 0$. When the system becomes unstable, γ changes sign from negative to positive. The Re at which this sign change occurs is referred as critical Reynolds number.

The objective here is to solve Eqs. (3) and (4) numerically. For this purpose, simulation is performed for $Re = 49$ (above the Re_{cr}). The transverse velocity signals at different locations along the flow axis in the downstream are monitored. Variations of instantaneous amplitude and frequency with respect to time should be extracted first from these signals. A Complex Demodulation Technique[35] (CDT) is used to extract the envelope and frequency domain of a given signal. In CDT, a complex signal is generated first. This complex signal contains the original signal information as its real part and the Hilbert transform of original signal as its imaginary part. The absolute value of the generated complex signal gives the instantaneous amplitude (envelope of the signal). Taking argument for the generated complex signal results in instantaneous phase. Differentiation of phase with respect to time gives the instantaneous frequency variation with time. Figure 10(a) shows the signal and its envelope. The oscillations observed in the curve is due to the boundary conditions related to CDT. However, these oscillations are small and become negligible as only the derivative of the envelope is considered for the further analysis. The extracted frequency domain using the complex demodulation technique for this signal is depicted in Figure 10(b).

Once the instantaneous values of amplitude and frequency is known, the plots of $d(\ln(\Lambda))/dt$ vs Λ^2 and St vs Λ^2 can easily be obtained by performing least square fit on the data points. These are shown in Figure 11 . The results of least square fit (slope and intersects) give the values of constants γ, α, ω, and β. In Figures 11(a) and 11(b), different lines resemble different sampling locations. The calculated values of these constants at different downstream locations are tabulated in Table IV. The last two columns of Table IV represent the constant of saturation (c_∞) and the angular frequency at saturation ($\Delta\omega$). c_∞ is defined as the ratio of β/α and $\Delta\omega$ is given as $\Delta\omega = -c_\infty\gamma$. From the table, it can be seen that the amplification rate (γ), the angular frequency (ω), and the variation of

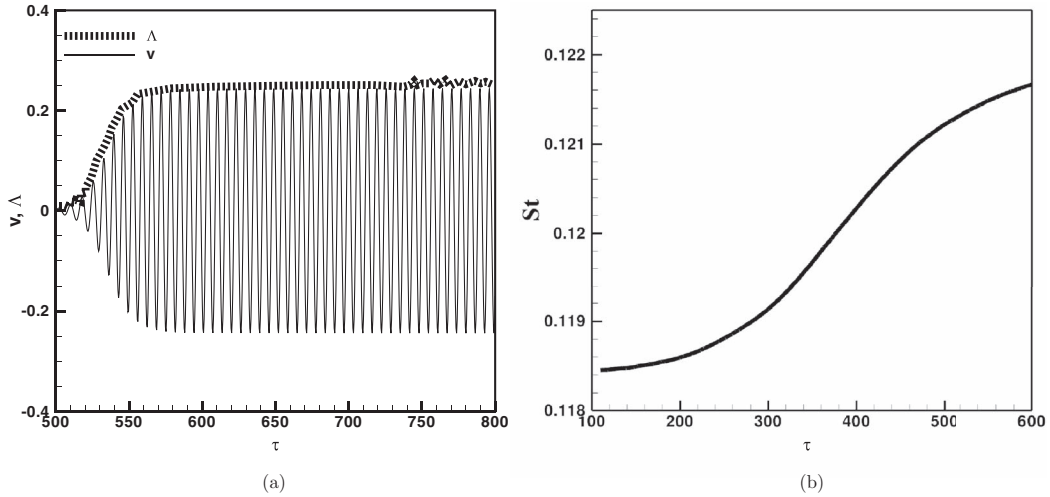

(a) (b)

FIG. 10. Complex demodulation technique applied to a signal: (a) Instantaneous amplitude, (b) instantaneous frequency.

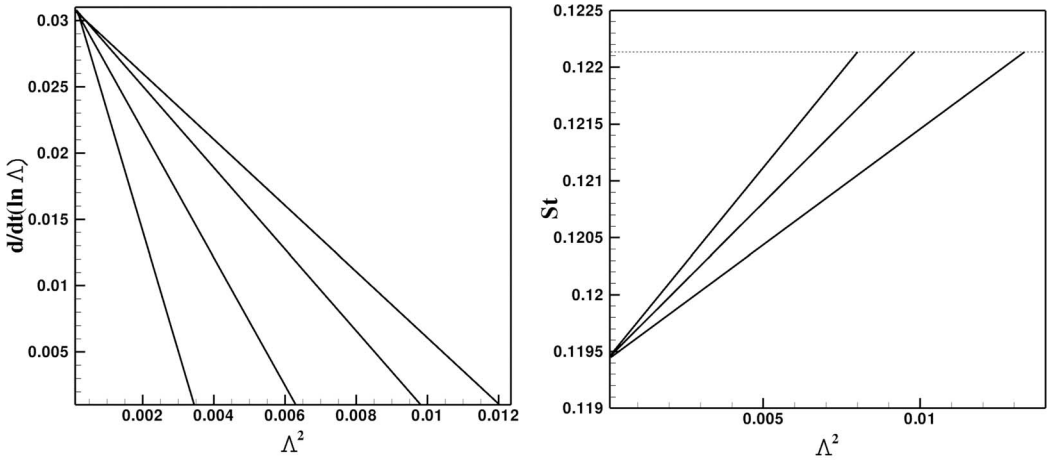

(a) (b)

FIG. 11. (a) Plot between $d(\ln(\Lambda))/dt$ and Λ^2, (b) plot between St and Λ^2.

TABLE V. Comparison of calculated Landau constants with the literature.

Reference	γ	ω	c_∞	$\Delta\omega$
Dušek *et al.*[5]	0.007931	0.7411	−2.709	0.02144
Kumar and Biswas[12]	0.011434	0.8341	−1.817	0.01967
Present	0.007414	0.8130	−2.381	0.01874

angular frequency at saturation ($\Delta\omega$) are identical at all the points considered for this study. This shows that the constants γ and ω are global in nature. On the other hand, Table IV also reveals that α and β are not identical in all the points and hence they are not constants. The necessary condition for an amplitude to grow is that the value of α should be high so that amplification at saturation is small. This is observed in Table IV. From this, it can be understood that Landau constants predict the super-critical Hopf bifurcation. The Landau constants calculated in this study are compared with the previous works (Table V) and found to be in good agreement with the literature values.

TABLE VI. Variation of γ and ω with respect to Re for flow past circular cylinder.

Re	γ	ω
48	−0.004	0.8120
49	0.0074	0.8128
50	0.0148	0.8132
51	0.0242	0.8136
52	0.0336	0.8139
53	0.0430	0.8141

TABLE VII. Variation of γ and ω with respect to Re for flow the case of AR = 0.4 and AOA = 60°.

Re	γ	ω
30	−0.0152	0.6883
31	−0.0039	0.6889
32	0.0097	0.6903
33	0.0218	0.6908
34	0.0347	0.6912
35	0.0475	0.6917

The same method is extended to calculate Re_{cr} and St_{cr}. Here, the simulations are carried out for a range of Re given as $Re_{cr} \pm \Delta Re$, where $\Delta Re \neq 0$. For circular cylinder, the simulations are performed for $Re = 48$, 49, 50, 51, 52, and 53. The transverse velocity signal at the particular point in the computational domain or the lift signal is taken for calculating the Landau constants. Table VI gives the values of γ and ω obtained for different Re. It is known that the Hopf bifurcation occurs when the sign of γ changes from negative to positive. Therefore, the Re at which γ becomes zero gives the value of Re_{cr}. A least square curve fit on the data gives Re_{cr} as 48.325 which is in good agreement with the literature.[5] The St_{cr} is found out to be 0.1221 from Figure 11(b). Calculation of Landau constants and thus estimating Re_{cr} and St_{cr} from them is performed for all the cases considered in this study and one such example for the case of elliptic cylinder of AR = 0.4 kept at AOA = 60° is reported in Table VII .

VII. A COMPARATIVE ANALYSIS

The above explained and validated techniques are now applied to all the combinations of AR and AOA considered in this study. The comparison of results is given in Table VIII. From the table, it can be understood that all these three methods predict the same Re_s and Re_{cr} with only a marginal difference.

VIII. EFFECT OF AXIS RATIO AND ANGLE OF ATTACK

The computed values of Re_s, Re_{cr}, and St_{cr} are given in Table VIII. This table is used to discuss the effect of thickness and incidence on onset of laminar separation and vortex shedding Reynolds numbers.

It is observed that Re_s maintains an inverse relationship with AR when AOA $\leq 45°$. This observation proves that as the body becomes slender to bluff, the tendency of fluid to separate increases. However, this trend is limited to smaller incidence. A direct relationship between Re_s and AR is discovered for AOA $\geq 60°$. This trend is attributed to the physical fact that when the incidence is high, the stagnation point moves away from the edges, and thus the fluid has to pass through a sudden upheaval upon contacting the body surface. This sudden upheaval causes the loss of momentum in fluid which leads to separation. However, when the thickness increases, the length of

TABLE VIII. Comparison of Re_s and Re_{cr} obtained by different methods and computed St_{cr} values. (FVM – Flow Visualization Method, WLM – Wake Length Method, FSCM – Flow Separation Criteria Method, SAA – Saturation Amplitude Analysis, HBA – Hopf Bifurcation Analysis, NA – Not Applicable.)

			Re_s			Re_{cr}			St_{cr}
Flow no.	AR	AOA (deg)	FVM	WLM	FSCM	FVM	SAA	HBA	HBA
1	0.1	0	437.5±0.5	437.18	437.311	512.5±0.5	512.21	512.284	0.4132
2	0.1	30	21.5±0.5	NA	21.132	68.5±0.5	68.44	68.411	0.1709
3	0.1	45	9.5±0.5	NA	9.121	35.5±0.5	35.21	35.184	0.1037
4	0.1	60	2.5±0.5	NA	2.018	27.5±0.5	27.15	27.247	0.1023
5	0.1	90	0.5±0.5	0.90	0.814	23.5±0.5	23.48	23.468	0.0971
6	0.4	0	12.5±0.5	12.68	12.628	231.5±0.5	231.38	231.415	0.2181
7	0.4	30	14.5±0.5	NA	14.005	63.5±0.5	63.42	63.455	0.1587
8	0.4	45	8.5±0.5	NA	8.781	36.5±0.5	36.08	36.112	0.1107
9	0.4	60	3.5±0.5	NA	3.213	31.5±0.5	31.29	31.287	0.1098
10	0.4	90	2.5±0.5	2.31	2.332	28.5±0.5	28.50	28.540	0.1077
11	0.6	0	8.5±0.5	8.28	8.125	87.5±0.5	87.57	87.567	0.1824
12	0.6	30	11.5±0.5	NA	11.811	56.5±0.5	56.44	56.444	0.1465
13	0.6	45	8.5±0.5	NA	8.081	37.5±0.5	37.04	37.118	0.1180
14	0.6	60	4.5±0.5	NA	4.189	34.5±0.5	34.37	34.398	0.1120
15	0.6	90	3.5±0.5	3.11	3.347	31.5±0.5	31.34	31.008	0.1104
16	0.8	0	7.5±0.5	7.12	7.081	64.5±0.5	64.21	64.208	0.1579
17	0.8	30	9.5±0.5	NA	9.843	53.5±0.5	53.98	53.957	0.1342
18	0.8	45	7.5±0.5	NA	7.614	38.5±0.5	38.84	38.711	0.1186
19	0.8	60	5.5±0.5	NA	5.204	37.5±0.5	37.36	37.384	0.1159
20	0.8	90	5.5±0.5	5.08	4.977	36.5±0.5	36.26	36.215	0.1121
21	1.0	...	6.5±0.5	6.27	6.738	48.5±0.5	48.34	48.325	0.1221

surface along which the fluid travels increases, and it gives ample opportunity for the fluid to regain its momentum. This is why Re_s exhibits a direct relationship with AR for higher AOA. Therefore, it is clear that the variation of Re_s with respect to AR depends on AOA. It is also found out that there exists a critical AOA, essentially in between 45° and 60° for which the relationship between Re_s and AR changes from inverse to direct. Increase in Re_s with respect to AR at AOA = 90° is in good agreement with the earlier observations of Park *et al.*[29]

The effect of AOA on Re_s can be seen in Table VIII. Re_s exhibits both monotonic and non-monotonic behavior with AOA for a given AR. For any AR except AR = 0.1, upon increase in AOA, Re_s increases till 30°, and then it decreases. This kind of non-monotonic behavior is also reported by Sen *et al.*[2] However, monotonic decrease in Re_s is observed for increasing AOA at AR = 0.1. This kind of monotonic behavior of Re_s is not reported in the literature. As a result, this study concludes that change in Re_s with respect to AOA depends on AR which is contradictory from previous observations.

In the case of Re_{cr} and St_{cr}, they keep an inverse relationship with AR for AOA $\leq$ 30°. However, Re_{cr} and St_{cr} maintain a direct relationship with AR for AOA $\geq$ 45°. Consequently, variation of Re_{cr} and St_{cr} with respect to AR depends on AOA.

The effect of increasing the AOA results decrease in Re_{cr} and St_{cr} for any given AR. Therefore, the variation of Re_{cr} and St_{cr} with respect to AOA is completely independent of AR. The variation also shows that as AOA is increased, the Hopf bifurcation occurs at small Re, however with a less perturbation frequency.

IX. FUNCTIONAL RELATIONSHIP

Finally, functional relationships are obtained for Re_s, Re_{cr}, and St_{cr} as a function of AR and AOA. In order to keep the equations in fully non-dimensional form, a variable λ = AOA/90° is defined as a non-dimensional quantity for AOA. These correlations are valid for 0 $\leq$ AR $\leq$ 1 and 0°

TABLE IX. Comparison of obtained St_{cr} values between simulation and correlation equation.

AR	AOA (deg)	Values obtained through HBA	Values obtained by Eq. (7)	% error
0.1	30	0.171	0.157	− 14.8
0.4	45	0.110	0.122	10.9
0.6	60	0.112	0.118	5.4
0.8	90	0.112	0.128	14.2
1.0	...	0.122	0.124	1.63

$\leq$ AOA $\leq 90^{\circ}$. The functional form for Re_s, Re_{cr}, and St_{cr} are given as

$$Re_s = 6.574AR^{(-2.032\lambda^2+4.811\lambda-1.881)}, \tag{5}$$

$$Re_{cr} = 43.513AR^{(-1.920\lambda^2+3.197\lambda-1.023)}, \tag{6}$$

$$St_{cr} = 0.124AR^{(-0.899\lambda^2+1.476\lambda+0.493)}. \tag{7}$$

The values of Re_s, Re_{cr}, and St_{cr} obtained through correlation equations are compared with the numerical results and one such example is shown in Table IX for St_{cr}. The average percentage error between the correlation and simulation values is $\pm 15\%$.

X. CONCLUSIONS

This paper is aimed to study the onset of flow separation and vortex shedding in flow past unconfined two-dimensional elliptic cylinders of various AR and AOA. Diverse methods including a stability analysis to study the Hopf bifurcation are used to estimate Re_s, Re_{cr}, and St_{cr}. The Landau equations are again proved to be necessary to analyze super-critical Hopf bifurcations. Typical Hopf constants for circular cylinder are estimated and compared with the available literature. The values of Re_{cr} and St_{cr} are found to be decreasing when AOA is increased. On the other hand, when AR increases the nature of variation for Re_s, Re_{cr} and St_{cr} are found to be dependent on AOA. Functional relationships are proposed for Re_{cr} and St_{cr} with respect to AR and AOA. This is the first ever reported study that deals with prediction of Re_{cr} and St_{cr} for flow past unconfined elliptic cylinders of various AR and AOA.

ACKNOWLEDGMENTS

The authors gratefully acknowledge the excellent computing facilities provided by High Performance Computing Center of IIT Madras. They also acknowledge the anonymous referees for their insightful comments which magnificently increased the quality of this article. I.P. acknowledges the help from Mrs. Mahalakshmi, a Research Scholar in Applied Mechanics department who helped him to learn complex demodulation technique.

[1] P. Drazin, *Introduction to Hydrodynamic Stability* (Cambridge University Press, Cambridge, 2002).
[2] S. Sen, S. Mittal, and G. Biswas, "Steady separated flow past elliptic cylinders using a stabilized finite-element method," Comput. Model Eng. Sci. **86**, 1–28 (2012).
[3] B. Zielinska, S. Goujon-Durand, J. Dusek, and J. Wesfreid, "Strongly nonlinear effect in unstable wakes," Phys. Rev. Lett. **79**, 3893 (1997).
[4] A. Lankadasu and S. Vengadesan, "Onset of vortex shedding in planar shear flow past a square cylinder," Int. J. Heat Fluid Flow **29**, 1054–1059 (2008).
[5] J. Dušek, P. L. Gal, and P. Fraunié, "A numerical and theoretical study of the first Hopf bifurcation in a cylinder wake," J. Fluid Mech. **264**, 59–80 (1994).
[6] K. Sreenivasan, P. Strykowski, and D. Olinger, "Hopf bifurcation, Landau equation, and vortex shedding behind circular cylinders," in Forum on Unsteady Flow Separation, edited by K.N. Ghia (American Society for Mechanical Engineers, Fluids Engineering Division, New York, 1987), Vol. 52, pp. 1–13.
[7] E. Berger and R. Wille, "Periodic flow phenomena," Annu. Rev. Fluid Mech. **4**, 313–340 (1972).
[8] M. Coutanceau and R. Bouard, "Experimental determination of the main features of the viscous flow in the wake of a circular cylinder in uniform translation. Part 1. Steady flow," J. Fluid Mech. **79**, 231–256 (1977).

[9] C. Williamson, "Oblique and parallel modes of vortex shedding in the wake of a circular cylinder at low Reynolds numbers," J. Fluid Mech. **206**, 579–627 (1989).
[10] C. Norberg, "An experimental investigation of the flow around a circular cylinder: Influence of aspect ratio," J. Fluid Mech. **258**, 287–316 (1994).
[11] C. Jackson, "A finite-element study of the onset of vortex shedding in flow past variously shaped bodies," J. Fluid Mech. **182**, 23–45 (1987).
[12] N. Kumar and G. Biswas, "A finite element study of the onset of vortex shedding in a flow past two-dimensional circular cylinder," Prog. Comput. Fluid. Dyn. Int. J. **8**, 288–298 (2008).
[13] B. Kumar and S. Mittal, "Prediction of the critical Reynolds number for flow past a circular cylinder," Comput. Methods Appl. Mech. Eng. **195**, 6046–6058 (2006).
[14] A. Sohankar, C. Norberg, and L. Davidson, "Low-Reynolds-number flow around a square cylinder at incidence: Study of blockage, onset of vortex shedding and outlet boundary condition," Int. J. Numer. Methods Fluids **26**, 39–56 (1998).
[15] B. Kumar and S. Mittal, "Effect of blockage on critical parameters for flow past a circular cylinder," Int. J. Numer. Methods Fluids **50**, 987–1001 (2006).
[16] A. Radi, M. C. Thompson, J. Sheridan, and K. Hourigan, "From the circular cylinder to the flat plate wake: The variation of Strouhal number with Reynolds number for elliptical cylinders," Phys. Fluids **25**, 101706 (2013).
[17] Y. Sudhakar and S. Vengadesan, "Vortex shedding characteristics of a circular cylinder with an oscillating wake splitter plate," Comput. Fluids. **53**, 40–52 (2012).
[18] S. Raman, K. Arul Prakash, and S. Vengadesan, "Effect of axis ratio on fluid flow around an elliptic cylinder: A numerical study," J. Fluids Eng. **135**, 111201 (2013).
[19] S. Raman, K. Arul Prakash, and S. Vengadesan, "Natural convection from a heated elliptic cylinder with a different axis ratio in a square enclosure," Numer. Heat Transfer, Part A **62**, 639–658 (2012).
[20] I. Paul, K. Arul Prakash, and S. Vengadesan, "Forced convective heat transfer from unconfined isothermal and isoflux elliptic cylinders," Numer. Heat Transfer, Part A **64**, 648–675 (2013).
[21] S. Dennis and G.-Z. Chang, "Numerical solutions for steady flow past a circular cylinder at Reynolds numbers up to 100," J. Fluid Mech. **42**, 471–489 (1970).
[22] S.-Y. Tuann and M. D. Olson, "Numerical studies of the flow around a circular cylinder by a finite element method," Comput. Fluids **6**, 219–240 (1978).
[23] A. Thom, "The flow past circular cylinders at low speeds," Proc. R. Soc. London, Ser. A **141**, 651–669 (1933).
[24] F. Homann, "Der einfluss grosser zähigkeit bei der strömung um den zylinder und um die kugel," Z. Angew. Math. Mech. **16**, 153–164 (1936).
[25] M.-H. Wu, C.-Y. Wen, R.-H. Yen, M.-C. Weng, and A.-B. Wang, "Experimental and numerical study of the separation angle for flow around a circular cylinder at low Reynolds number," J. Fluid Mech. **515**, 233–260 (2004).
[26] C. Norberg, "Flow around a circular cylinder: Aspects of fluctuating lift," J. Fluid. Struct. **15**, 459–469 (2001).
[27] I. Paul, "Effect of axis ratio and incidence on fluid flow and heat transfer around elliptic cylinders," Master's thesis (Indian Institute of Technology Madras, Chennai, 2013).
[28] I. Paul, K. Arul Prakash, and S. Vengadesan, "Numerical analysis of laminar flow past elliptic cylinders: A parametric study," Int. J. Numer. Method. H. (in press).
[29] J. K. Park, S. O. Park, and J. M. Hyun, "Flow regimes of unsteady laminar flow past a slender elliptic cylinder at incidence," Int. J. Heat Fluid Flow **10**, 311–317 (1989).
[30] S. Sen, S. Mittal, and G. Biswas, "Steady separated flow past a circular cylinder at low Reynolds numbers," J. Fluid Mech. **620**, 89–119 (2009).
[31] K. Srinivasan, "On a separation criterion for symmetric elliptic bluff body flows," e-print arXiv:physics/0511250 [physics.flu-dyn].
[32] A. Perry, M. Chong, and T. Lim, "The vortex-shedding process behind two-dimensional bluff bodies," J. Fluid Mech. **116**, 77–90 (1982).
[33] C. Mathis, M. Provansal, and L. Boyer, "The Benard-von Karman instability: An experimental study near the threshold," J. Phys. Let. (Paris) **45**, 483–491 (1984).
[34] L. Landau, *Fluid Mechanics*, Course Of Theoretical Physics Vol. 6 (Butterworth-Heinemann, Oxford, 1987).
[35] P. Le Gal, "Complex demodulation applied to the transition to turbulence of the flow over a rotating disk," Phys. Fluids **4**, 2523–2528 (1992).